第45卷第10期 中国科学技术大学学报 Vol. 45, No. 10
2015年10月 JOURNAL OF UNIVERSITY OF SCIENCE AND TECHNOLOGY OF CHINA Oct. 2015

文章编号:0253-2778(2015)10-0855-09

Power measurement based on VSLMS improved adaptive filters

QIAN Qi[1], KANG Yu[1,2*], ZHAO YunBo[3]

(1. *Department of Automation, University of Science and Technology of China, Hefei 230027, China*;
2. *State Key Laboratory of Fire Science, University of Science and Technology of China, Hefei 230027, China*;
3. *Department of Automation, Zhejiang University of Technology, Hangzhou 310014, China*)

Abstract: A new algorithm is proposed to detect and extract in real-time signals with fundamental and harmonic wave components in the power grid, which is applicable to power measurement. The proposed method is based on the concept of adaptive filter, and adaptively decomposes the measured power signal into its constituting components, resulting in a fast convergence rate. The fundamental and harmonic wave components in the power grid can be decomposed into a series of sinusoidal signals. The frequency of the power grid is measured by energy operator. A model of voltage and current wave in the power grid is constructed, a new step-size LMS algorithm for improving the adaptive filter is proposed and the stability of the proposed method is discussed. The effectiveness of the proposed method is demonstrated by simulation examples.

Key words: Adaptive filter; Power measurement; Fundamental and harmonic wave

CLC number: TP18 **Document code**: A doi: 10.3969/j.issn.0253-2778.2015.10.008

Citation: QIAN Qi, KANG Yu, ZHAO YunBo. Power measurement based on VSLMS improved adaptive filters[J]. Journal of University of Science and Technology of China, 2015, 45(10): 855-863.
钱其,康宇,赵云波. 基于改进的变步长自适应滤波算法的功率测量[J]. 中国科学技术大学学报, 2015, 45(10): 855-863.

基于改进的变步长自适应滤波算法的功率测量

钱 其[1],康 宇[1,2],赵云波[3]

(1. 中国科学技术大学自动化系,安徽合肥 230027; 2. 火灾科学国家重点实验室,中国科学技术大学,安徽合肥 230027;
3. 浙江工业大学自动化系,浙江杭州 310014)

摘要:基于自适应滤波,提出一种新的算法用于实时抽取电网中的基波和谐波信号,该算法能自适应地将被测量的电网信号分解成单个分量且具有很快的收敛速度,也能够进行功率测量.电网中的基波和谐波分量可以被分解成一系列正弦信号,可用能量算子来测量电网的频率.构建电网的电压和电流模型时,一个新的变步长 LMS 算法被用来改善自适应滤波器的速度,同时也证明了所提算法的稳定性。最后,用一个仿真实例说明了该算法的有效性.

关键词:自适应滤波;功率测量;基波和谐波

Received: 2015-03-06; **Revised**: 2015-04-16

Foundation item: Supported by the National Natural Science Foundation of China (61422307, 61304048 and 61174061), the Scientific Research Staring Foundation for the Returned Overseas Chinese Scholars of Ministry of Education of China and the National High-tech R&D Program of China (863)(2014AA06A503). the Youth Innovation Promotion Association, Chinese Academy of Sciences and National Youth Top Talent Support of National High-Level Personnel of Special Support Program.

Biography: QIAN QI, male, born in 1989. Research field: Control theory. E-mail: qqianl@mail.ustc.edu.cn
Corresponding author: Kang Yu, PhD/professor, E-mail: kangduyu@ustc.edu.cn

0 Introduction

In recent years, electrical harmonic pollution is becoming increasingly serious due to the extensive use of nonlinear components in electric devices. It has become a threat to power system by deteriorating the quality of electric energy and the safe and economical operation of power systems. Hence, accurate parameter measurement becomes important for the control and protection of the power grid. The large-scale nonlinear loads of the grid in modern power transmission can cause severe harmonic pollution as well as deviation from the grid frequency normally about 50Hz. Therefore, the measurement of the grid power in the presence of nonlinear loads disturbance becomes a severe challenge.

A great number of techniques have been proposed to analyze harmonics, including the fast Fourier transform (FFT); the phase-lacked-loop technique; wavelet transform and artificial neural networks in power system measurements, etc. However, FFT is accurate only when the sampling theorem is satisfied and sampling frequency is synchronized with the analog signal frequency (i. e., integer number of samples in an integer number of cycles). The synchronized sampling is merely theoretical, because of either the practical requirement of processing finite-duration records or unknown fluctuations of the input analog signal frequency. When sampling frequency is not synchronized with the concerned analog signal frequency, error arises because of the well-known leakage effect and grid effect. Generally speaking, the FFT method can lead to spectrum leakage and the veracity is based on the length of the measured power signal. This unavoidably decreases the accuracy between the real and the reference signals, thus making accurate measurement of power grid signal unattainable. The error is escalated under dynamic states, especially if there are harmonics or fluctuations in the amplitude of the signal. As a result, the errors in the frequency estimation may become too large. In [1], several window functions based on the FFT method were compared and a polynomial approximation method was proposed to further reduce leakage and noise interference. In[2], the leakage phenomenon of FFT was discussed and a new algorithm, poly-item cosine window interpolation, was proposed to reduce the leakage and constrain the interference among harmonics and noises. However, the interpolation algorithm based on windowing FFT was too time-consuming to be used on-line due to requirements of large number of samples and the difficulty in solving the interpolation equation.

Other methods also have their deficiencies. Methods based on ANF were very complex and difficult to implement in practice[3, 5], with an unverified influence between adaptive notch filters. The band-pass filter required a high order for measurement accuracy, which thus posed challenges to the computational resources as well as the distortion signal due to the additional phase shift effect[6]. The characteristic of wavelet transform and neural network methods was difficult computation for real-time implementation[7-12]. The cut off frequency of low-pass filter in PLL (Phase Locked Loop) was set relatively low in order to achieve good filtering. However, the low cut off frequency affected the dynamic characteristics of the detection system.

In this work, a new method is proposed to extract in realtime the fundamental wave and every harmonic wave in-time without knowing the frequency of the power grid a priori. The method has a simple structure and can be readily implemented in practice. The energy operator is applied to estimate the frequency of the power grid. We verify the effectiveness by both theoretical analysis and numerical simulations.

2 Model of fundamental and harmonic ware

A distorted current or voltage wave can be expanded into Fourier series[13], as follows,

$$i(t) = \sum_{h=1}^{\infty} I_h \sin(h\omega_o t + \phi_h) \quad (1)$$

$$v(t) = \sum_{h=1}^{\infty} V_h \sin(h\omega_o t + \theta_h) \quad (2)$$

where I_h is the h-th peak harmonic current, v_h is the h-th peak harmonic voltage, ϕ_h and θ_h are h-th harmonic current and voltage phase, respectively, and ω_o is the angular frequency of the fundamental wave. The above equations can be transformed to

$$i(t) = \sum_{h=1}^{\infty} i_h(t) \quad (3)$$

$$v(t) = \sum_{h=1}^{\infty} v_h(t) \quad (4)$$

where $i_h(t) = I_h \sin(h\omega_0 t + \varphi_h)$, $v_h = V_h \sin(h\omega_0 t + \theta_h)$. When $h = 1$, $i_h(t)$ and $v_h(t)$ are the fundamental current and voltage, respectively.

The distorted factor of voltage is defined as the total harmonic distortion of voltage THD_v, which can be calculated as follows,

$$\mathrm{THD}_v = \frac{1}{V_1}\sqrt{\sum_{h=2}^{\infty} V_h^2} = \sqrt{\frac{V_{\mathrm{rms}}}{V_{1\,\mathrm{rms}}}^2 - 1} \quad (5)$$

where V_1 is the peak value of the fundamental wave, $V_{1\,\mathrm{rms}} = V_1$ and $V_{\mathrm{rms}} = \sqrt{\sum_{h=1}^{\infty} V_{h\,\mathrm{rms}}^2}$. Therefore, a voltage or current signal of the power grid can be decomposed into many integer frequency components, i.e. $V(t) = v_1 + v_2 + \cdots + v_h + \cdots$, $I(t) = i_1 + i_2 + \cdots + i_h + \cdots$, $h = 1, 2, \cdots$.

For an unsteady distort signal, the power grid model can be reduced as in Fig. 1.

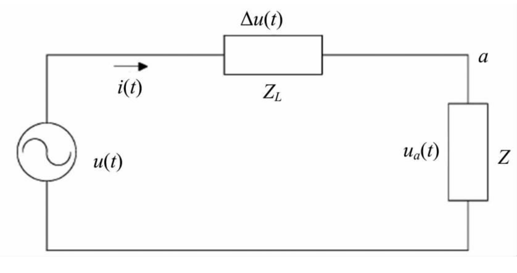

Fig. 1 Reduced model of the power grid

The voltage and current can be written as follows:

$$u_a(t) = u_1(t) + u_d(t) \quad (6)$$

$$i(t) = i_1(t) + i_d(t) \quad (7)$$

where $u_1(t)$ and $u_d(t)$ are the fundamental and distorted wave voltage, respectively, and $i_1(t)$ and $i_d(t)$ are the fundamental and distorted wave current, respectively.

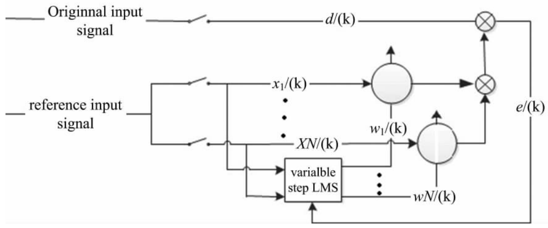

Fig. 2 Schematic diagram of the filter

Based on the power theory, instantaneous power can be obtained as follows:

$$p_a(t) = u_a(t) \times i(t) \quad (8)$$

and then

$$\begin{aligned} p_a(t) &= [u_1(t) + u_d(t)][i_1(t) + i_d(t)] = \\ & u_1(t)i_1(t) + u_1(t)i_d(t) + u_d(t)i_1(t) + u_d(t)i_d(t) \\ &= p_1(t) + p_{1d}(t) + p_{d1}(t) + p_d(t) \end{aligned} \quad (9)$$

Thus, the mean power is

$$\begin{aligned} P_a &= \frac{1}{T}\int_0^T p_a(t)\,\mathrm{d}t = \\ & \frac{1}{T}\int_0^T [p_1(t) + p_{1d}(t) + p_{d1}(t) + p_d(t)]\mathrm{d}t = \\ & P_1 + P_{1d} + P_{d1} + P_d \end{aligned} \quad (10)$$

where P_1, P_{1d}, P_{d1} and P_d are the fundamental wave power, power generated by fundamental wave voltage and distorted wave current, power generated by distorted wave voltage and fundamental wave current and power generated by distorted wave voltage and distorted wave current, respectively. P_d is also referred to as the distorted power.

By the analysis of the power trend direction, the following conclusions can be acquired: $P_1 > 0$, i.e., the fundamental wave power is positive; $P_{1d} \geqslant 0$, i.e., the power generated by fundamental wave voltage and distorted wave current is non-negative; $P_{d1} \leqslant 0$, i.e., the power generated by distorted wave voltage and fundamental wave current is non-positive; and $P_d < 0$, i.e., the distorted power is negative. Therefore the reasonable grid power P can be calculated as follows,

$$\begin{aligned} P &= P_1 + P_{1d} + P_{d1} + P_d = \\ & (P_1 + P_{1d} + P_{d1} + P_d + P_d) - P_d = \end{aligned}$$

$$P_a - P_d \tag{11}$$

where P_a is real measure power of a system and P_d is the distorted power. The above equation is the foundation of the analysis in this work.

3 Design of the adaptive filter based on variable step-size LMS

It is proposed that a new adaptive filter based on a variable step LMS, the structure of which is shown in Fig. 2. After sampling the original input signal, $d(k)$ can be obtained. The reference input signal contains h pure sine wave with h times frequency of current fundamental wave, dispersed into $x_1(k), x_2(k), \cdots, x_h(k)$. $w_1(k)$, $w_2(k), \cdots, x_h(k)$ are weight values with two free degrees. Therefore after the combination of sine wave amplitude and phase angle, it is easy to keep the original input amplitude and phase angle $d(k)$ and reference input $y(k)$ the same, that is, the final output $e(k)$ convergences to zero. We have

$$\left.\begin{aligned} &y(k) = \sum\nolimits_{h=1}^{N} w_h(k)x_h(k) \\ &e(k) = d(k) - y(k) \\ &u(k) = a \times [\sin(f \times j(e(k)j^2 - \pi/2) + 1] \\ &w_h(k+1) = w_h(k) + u(k)e(k)x(k) \end{aligned}\right\} \tag{12}$$

where $u(k) \subseteq \left[0, \frac{1}{\lambda_{\max}}\right)$ is the variable step-size, and $\lambda_{\max}$ is the largest eigenvalue of autocorrelation matrix of the input signal. Based on Eq. (12), we obtain

$$u(k) = a \times [\sin(f \times |\ (e(k)\ |^2 - \pi/2) + 1] \leqslant a \tag{13}$$

where w_0 is the desirable weight vector.
Then

$$\begin{aligned} &w(k+1) = w(k+1) - w_0 = \\ &w(k) + u(k)e(k)x(k) - w_0 = \\ &\Delta w(k) + u(k)e(k)x(k) \leqslant \\ &\Delta w(k) + ae(k)x(k) = \\ &\Delta w(k) + ax(k)[x(k)^{\mathrm{T}} w_0 + n(k) - \\ &x(k)Tw(k)] = \\ &\Delta w(k) + ax(k)[e_0(k) - x(k)^{\mathrm{T}} w(k)] = \\ &[I - ax(k)x^{\mathrm{T}}(k)]\Delta w(k) + ae_0(k)x(k) \end{aligned} \tag{14}$$

where $e_0(k)$ is the optimal output error, which can be written as:

$$\begin{aligned} &e_0(k) = d(k) - w_0^{\mathrm{T}}(k)x(k) = \\ &w_0^{\mathrm{T}} x(k) + n(k) - w_0^{\mathrm{T}} x(k) = n(k) \end{aligned} \tag{15}$$

where $n(k)$ is the measurement white noise with zero mean and the variance σ_n^2. This is an adaptive (time-varying) algorithm about the the discrete frequency response of the original adaptive filter. To analyze this, consider the averaged system corresponding to Eq. (14).

$$\begin{aligned} &e_0(k) = \boldsymbol{E}[\boldsymbol{I} - a\boldsymbol{x}(k)\boldsymbol{x}^{\mathrm{T}}(k)]\Delta w(k) + \\ &\boldsymbol{E}ae_0(k)\boldsymbol{x}(k) = \\ &[\boldsymbol{I} - a\boldsymbol{E}[\boldsymbol{x}(k)x^{\mathrm{T}}(k)]\boldsymbol{E}[\Delta w(k)] = \\ &[\boldsymbol{I} - a\boldsymbol{E}[\boldsymbol{x}(k)\boldsymbol{x}^{\mathrm{T}}(k)]]^{k+1}\boldsymbol{E}[\Delta w(0)] = \\ &(\boldsymbol{I} - a\boldsymbol{R})^{k+1}\boldsymbol{E}[\Delta w(0)] \end{aligned} \tag{16}$$

where $\boldsymbol{R} = \boldsymbol{E}[\boldsymbol{x}(k)\boldsymbol{x}^{\mathrm{T}}(k)]$.

$$\begin{aligned} &\boldsymbol{E}[\boldsymbol{Q}^{\mathrm{T}} w(k+1)] = (\boldsymbol{I} - a\boldsymbol{Q}^{\mathrm{T}}\boldsymbol{R}\boldsymbol{Q}) \times \boldsymbol{E}[\boldsymbol{Q}^{\mathrm{T}}\Delta w(k)] \\ &= \boldsymbol{E}[\Delta w'(k+1)] = \boldsymbol{A} \times \boldsymbol{E}[\Delta w'(k)] \\ &= \boldsymbol{A}^{k+1}\boldsymbol{E}[w'(0)] \end{aligned} \tag{17}$$

where,

$$\boldsymbol{A} = \begin{bmatrix} 1 - a\boldsymbol{\lambda}_0 & 0 & \cdots & 0 \\ 0 & 1 - a\boldsymbol{\lambda}_1 & \cdots & \vdots \\ \vdots & \vdots & \cdots & \vdots \\ 0 & 0 & \cdots & 1 - a\boldsymbol{\lambda}_N \end{bmatrix}$$

$\boldsymbol{Q}$ is the diagonalizable matrix of $\boldsymbol{R}$, $\boldsymbol{Q}^{\mathrm{T}} w(k) = \Delta w'(k)$. Then Eg. (17) can be written as:

$$\boldsymbol{E}[\Delta w'(k+1)] = \boldsymbol{A}^{k+1}\boldsymbol{E}[\Delta w'(0)] \tag{18}$$

In order to ensure the convergence of $\Delta w'(k+1)$, $|1 - a\lambda_n| < 1$, so $0 \leqslant a < \frac{1}{\lambda_{\max}}$, $\lambda_{\max} = \max\{\lambda_n\}$, $n = 0, 1, 2, \cdots; N$, λ_n is the eigenvalue of the input signal autocorrelation matrix.

The convergence of the LMS algorithm requires that the step-size of LMS algorithm be within certain limits, i. e., $0 \leqslant a < \frac{1}{\lambda_{\max}}$

$u(k)$ is the factor controlling the convergence speed. To study the value change with variation of a and f, simulations have been done. As Fig. 3 shows, a has an important effect on the algorithm speed. The bigger a is, the larger the initial step is, and the faster the iteration speed. As Fig. 4

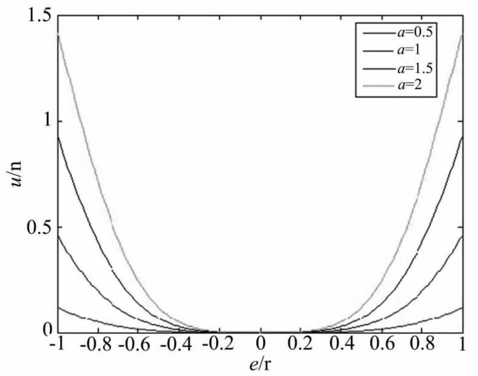

Fig. 3 $a=1$, as $e(n)$ changed, the curve of $\mu(n)$ along with the change of f

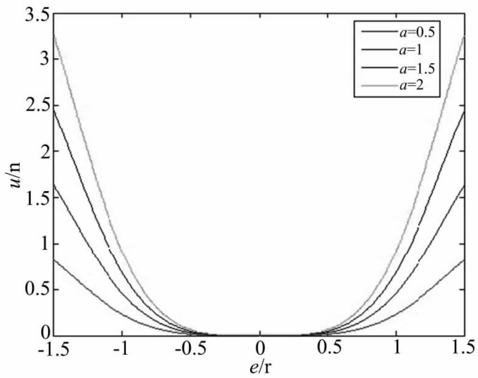

Fig. 4 $f=1$, as $e(n)$ changed, the curve of $\mu(n)$ along with the change of f

shows, f has an important effect on the way of convergence. A bigger f makes the convergence of $e(k)$ non-smooth. In addition, a should be appropriately selected for a stable result.

In the above design, the system arrives at the steady state, i. e. $e(k)\to 0$, $d(k)\to y(k)=\sum_{h=1}^{N} w_h(k)x_h(k)$. Thus every harmonic component can be extracted accurately, i. e. , $v_h(k)=w_h(k)\times x_h(k)$; $h=1,2,\cdots,N$, and then the harmonic distorted factor THD_V, THD_I, the fundamental wave power P_1 and the distorted power P_d can be calculated.

4 Frequency estimation of the signal in power grid

Energy operator can be used to calculate the frequency and amplitude for AM-FM. The energy separation algorithm (ESA) is a simple demodulating technique for AM-FM demodulation. It is less computationally complex and has better time resolution than other classical demodulation approaches such as the Hilbert transform.

4.1 Continuous-time

The teager energy operator, $\boldsymbol{\Psi}[\cdot]$, defined for continuoustime signal $\boldsymbol{x}(t)$ as follows, can track the energy and identify the instantaneous amplitude and frequency,

$$\begin{aligned} \boldsymbol{\Psi}[\boldsymbol{x}(t)] &= 2[\dot{\boldsymbol{x}}(t)]^2 - \boldsymbol{x}(t)\times\ddot{\boldsymbol{x}}(t) \\ \boldsymbol{\Psi}[\dot{\boldsymbol{x}}(t)] &= 2[\ddot{\boldsymbol{x}}t)]^2\dot{\boldsymbol{x}}(t)\times\dddot{\boldsymbol{x}}(t) \end{aligned} \tag{19}$$

where $\dot{\boldsymbol{x}}(t)$ and $\ddot{\boldsymbol{x}}(t)$ are the first and the second time derivatives of $\boldsymbol{x}(t)$, respectively.

An important aspect of teager energy operator is that it is almost instantaneous, because only three samples are required for the energy computation at each time instant. This excellent time resolution provides us with the ability to capture the energy fluctuations. Furthermore, this operator is very easy to implement efficiently. The ESA developed in Ref. [11] uses teager energy operator to separate $\boldsymbol{x}(t)$ into its amplitude envelope $|a(t)|$ and IF signal $f(t)$ to accomplish moncomponent AM-FM signal demodulation,

$$\left.\begin{aligned} &\boldsymbol{x}(t) = a(t)\times\sin(\omega\times t) \\ &\dot{\boldsymbol{x}}(t) = \dot{a}(t)\sin(\omega\times t) + a(t)\times\omega\times\cos(\omega\times t) \\ &\dot{\boldsymbol{x}}(t) = \ddot{a}(t)\sin(\omega\times t) + 2\omega\dot{a}(t)\omega\cos(\omega\times t) \\ &-\omega^2 a(t)\sin(\omega\times t) \\ &\dddot{x}\boldsymbol{x}(t) = \dddot{a}(t)\sin(\omega\times t) - \ddot{a}(t)\omega\,\omega\cos(\omega t) \\ &+2\ddot{a}(t)\cos(\omega t) - 2\omega 2\ddot{a}(t)\sin(\omega\times t) \\ &-\omega^2\dot{a}(t)\sin(\omega t) + 2\omega^3 a(t)\cos(\omega t) \\ &\dot{x}(t) = \dot{a}(t)\sin(\omega t+\theta) \\ &+\omega a(t)\cos(\omega\times t+\theta) = \boldsymbol{y}_1 + \boldsymbol{y}_2 \end{aligned}\right\} \tag{20}$$

Lemma 4.1[14] (Ⅰ) a and q are bandlimited with highest frequencies ω_a, and ω_f respectively, and ω_a, $\omega_f<\omega_c$.

(Ⅱ) $\omega_a^2+\omega_m\omega_f\leqslant(\omega_m+\omega_c)^2$ where $\int x(t)=a(t)\sin(\omega t+\theta)=a(t)\sin(\omega t+\omega_m\int_0^t q(t)\,\mathrm{d}t+\theta)$, $\omega_1=\dfrac{d(\omega_t+\theta)}{t}=\omega+\omega_m q(t)$. Further, if we define the order of magnitude of a signal z to be $O(z)=O(z_{\max})$ where $z_{\max}=\max_t z(t)$ **应改为** $z_{\max}=\max_t|z(t)|$, then $O(\boldsymbol{y}_1)\approx O(a\omega)$ and $O(\boldsymbol{y}_2)\approx O$

($a\omega_1$). Since $O(\omega) \ll O(\omega_1)$, by ignoring $\boldsymbol{y}_1$, we obtain the approximation:

$$\dot{\boldsymbol{x}}(t) \approx y_2 = a(t)\omega\cos(\omega t)$$

Hence,

$$\left.\begin{aligned} \ddot{\boldsymbol{x}}(t) &= -a(t)\omega^2\sin(\omega t) \\ \dddot{\boldsymbol{x}}(t) &= -a(t)\omega^3\cos(\omega t) \end{aligned}\right\} \tag{21}$$

Then

$$\begin{aligned} &\Psi[x(t)] = [\dot{x}(t)]^2 - x(t) \times \ddot{x}(t) = \\ &a(t)\omega\cos(\omega_t)]^2 - (a(t)\sin(\omega t)) \\ &(-a(t)\omega^2\sin(\omega_t)) = \\ &a^2(t)\omega^2(\cos^2(\omega t) + \sin^2(\omega t)) = \\ &a^2(t)\omega^2 \end{aligned} \tag{22}$$

$$\begin{aligned} &\Psi[\dot{x}(t)] = [\ddot{x}(t)]^2 - \dot{x}(t) \times \dddot{x}(t) = \\ &(-a(t)\omega^2\sin(\omega t))^2 - a(t)\omega\cos(\omega t) \times \\ &(-a(t)\omega^3\cos(\omega t)) = \\ &a^2(t)\omega^4(\sin^2(\omega t) + \cos^2(\omega t)) = \\ &a^2(t)\omega^4 \end{aligned} \tag{23}$$

Finally we obtain

$$|f(t)| \approx \frac{1}{2\times\pi}\sqrt{\frac{\boldsymbol{\Psi}[\dot{\boldsymbol{x}}(t)]}{\boldsymbol{\Psi}[\boldsymbol{x}(t)]}} \tag{24}$$

$$|a(t)| = \frac{\boldsymbol{\Psi}[\boldsymbol{x}(t)]}{\boldsymbol{\Psi}[\dot{\boldsymbol{x}}(t)]} \tag{25}$$

4.2 Discrete-time

In the discrete case, the time derivatives may be approximated by time differences. The discrete-time conterpart of Teager Energy Operator becomes

$$\begin{aligned} &\boldsymbol{\Psi}[\boldsymbol{x}(n)] = \\ &[\dot{\boldsymbol{x}}(n)]^2 - \boldsymbol{x}(n) * \ddot{\boldsymbol{x}}(n) = \\ &[\boldsymbol{x}(n+1) - \boldsymbol{x}(n)]^2 - \boldsymbol{x}(n) * [\dot{\boldsymbol{x}}(n+1) - \dot{\boldsymbol{x}}(n)] = \\ &\boldsymbol{x}^2(n+1) - 2 * \boldsymbol{x}(n+1)\,\boldsymbol{x}(n) + \boldsymbol{x}^2(n) - \\ &\boldsymbol{x}(n) * [\boldsymbol{x}(n+2) - \boldsymbol{x}(n+1) - \boldsymbol{x}(n+1) + \boldsymbol{x}(n)] = \\ &\boldsymbol{x}^2[n] - \boldsymbol{x}[n-1] * \boldsymbol{x}[n+1] \end{aligned} \tag{26}$$

Considering the fundamental wave signal in power grid, i.e. $\boldsymbol{x}(t) = \boldsymbol{A}\sin(\omega t + \theta)$,

$$\begin{aligned} \boldsymbol{\Psi}[\boldsymbol{x}(n)] &= \boldsymbol{x}^2[n] - \boldsymbol{x}[n-1] * \boldsymbol{x}[n+1] = \\ &(\boldsymbol{A} * sin\ (\omega * n + \theta))^2 - \\ &[\boldsymbol{A} * \sin(\omega * (n-1) + \theta)] * \\ &[\boldsymbol{A} * \sin(\omega * (n+1) + \theta)] = \\ &\boldsymbol{A}^2 \sin^2(\omega * n + \theta) - \boldsymbol{A}^2\sin(\omega * (n-1) + \theta) * \\ &\sin(\omega * (n+1) + \theta) = \\ &\boldsymbol{A}^2\,\omega^2\left(\frac{\sin(\Omega)}{\Omega}\right)^2 \end{aligned} \tag{27}$$

where $\Omega = \frac{\omega}{T}$ and T is the sample time.

The three-sample derivative is defined as $\boldsymbol{y}(n) = \boldsymbol{x}(n+1) - \boldsymbol{x}(n-1)$, thus

$$\begin{aligned} &\boldsymbol{\Psi}[\boldsymbol{y}(n)] = \boldsymbol{\Psi}[\boldsymbol{x}(n+1) - \boldsymbol{x}(n-1)] = \\ &\boldsymbol{\Psi}[\boldsymbol{A}\sin(\omega(n+1) + \theta) - \boldsymbol{A}\sin(\omega(n-1) = \\ &\boldsymbol{\Psi}[\boldsymbol{A}\cos(2\omega n + \theta)\sin(\omega)] = \\ &4\boldsymbol{A}^2\sin^2(\omega)\omega^2\left(\frac{\sin(\Omega)}{\Omega}\right)^2 \end{aligned} \tag{28}$$

Then, we obtain

$$\frac{\boldsymbol{\Psi}[y(n)]}{4\boldsymbol{\Psi}[x(n)]} = 1 - \cos(2\omega) \tag{29}$$

$$\begin{aligned} f &= \frac{1}{2*\pi} = \frac{1}{2*\pi}\arccos\left[1 - \frac{\boldsymbol{\Psi}[y(n)]}{4\boldsymbol{\Psi}[x(n)]}\right] = \\ &\frac{1}{4*\pi}\arccos\left[1 - \frac{\boldsymbol{\Psi}[y(n)]}{4\boldsymbol{\Psi}[x(n)]}\right] \end{aligned} \tag{30}$$

Eq. (30) is used to calculate the frequency of the signal in the power grid.

5 Simulation results

Since the third and seventh distorted components are large in the power grid, it is assumed that the voltage and current signal in the power grid are both polluted by the third and seventh distorted waves, i.e.,

$$\begin{aligned} V(t) &= 220\sin(2\times\pi f_0 t) + \\ &\quad 20\sin(2\times\pi 3 f_0 t) + 3\sin(2\times\pi 7 f_0 t), \\ I(t) &= 20\sin(2\times\pi f_0 t) \\ &\quad + 3\sin(2\times\pi 3 f_0 t) + 0{:}5\sin(2\times\pi 7 f_0 t); \end{aligned}$$

where the first component is the fundamental wave component, the second and third are the harmonic wave components of voltage (current), and $f_0 = 50$ is the frequency of the power signal. There is 10db additive white Gaussian noise in the voltage and current signal.

The frequency of voltage signals are calculated by Eq. (27). Through the low pass filter, the third and seventh distorted voltage waves are eliminated and the fundamental one can be obtained. The sampling frequency of the simulation is 2000Hz, i.e., $f_s = 2000\text{Hz}$. The order of the designed low pass filter is 128. The simulation result is shown in Fig. 5, where the frequency estimated by TEO is satisfactory.

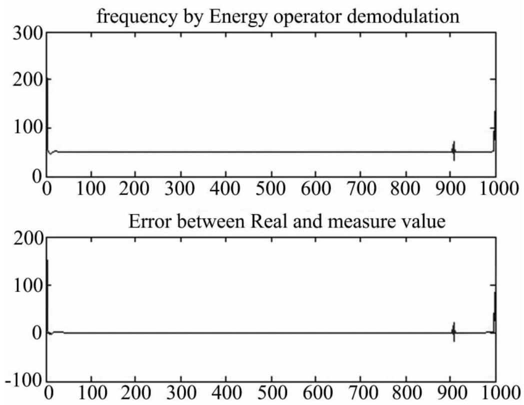

Fig. 5 Frequency of power signal

Compared with the fix-LMS and ws-LMS[15], the new adaptive filter based on the variable step LMS structure have the following parameters: (i) for the voltage signal, $w_1 = 0.1$, $w_2 = 0.1$, $w_3 = 0.1$, $a = 0.3$, $f = 40$; (ii) for the current signal, $w_1 = 0.1$, $w_2 = 0.1$, $w_3 = 0.1$, $a = 0.3$, $f = 29$. With simulations the new adaptive filter based on the fixed step LMS structure have the following parameters: (i) the parameters of the voltage signal, $w_1 = 0.1$, $w_2 = 0.1$, $w_3 = 0.1$, $u = 0.3$; (ii) the parameters of the current signal, $w_1 = 0.1$, $w_2 = 0.1$, $w_3 = 0.1$, $u = 0.3$. The simulation results are shown in Figs. 6～9.

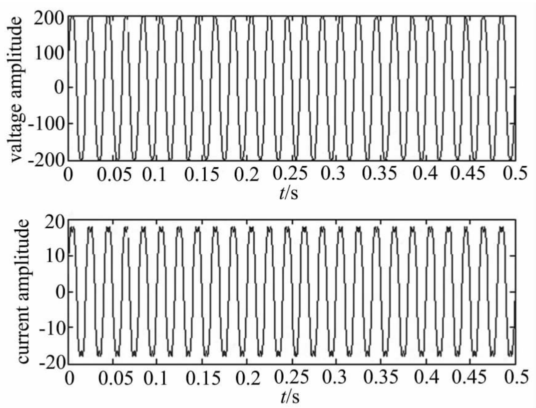

Fig. 6 Signal waveform of $V(t)$ and $I(t)$

In Fig. 6, we draw the waveform of the voltage and current signals which contain fundamental and harmonic wave components. Compared to the harmonic wave, the power measurement and distorted factors are more accurate. At the same time, the proposed method can effectively track and extract the signal with many different frequency harmonic waves in a power grid. With the proposed method, we can trace and check the fundamental and harmonic wave power and the distorted factors in real-time which shows the quality of a power grid.

From Figs. 6 ～ 9, compared to the filters based on fixed step LMS and wv-LMS, the proposed method can rapidly lead the system to the steady state at a higher accuracy. In Fig. 9, compared with the fix-LMS and wv-LMS, the proposed method shows good robustness against noise.

The fundamental wave and distorted power can be calculated as in Tabs. 1 and 2. We see that when the power grid signal contains fundamental wave and 3-th and 7-th harmonic waves, by using the proposed method, the error between the theoretical value and the measured one is -2.05×10^{-11} in the distorted power, and is 0 in fundamental power, much smaller compared to the power grid signal. This justifies the effectiveness of the proposed method.

6 Conclusion

A method for the detection and extraction of the components of a signal based on the concept of an adaptive filter is proposed. Its performance is evaluated in the context of the power grid signal. The method can accurately decompose the signal into its constituting components. Theoretical and

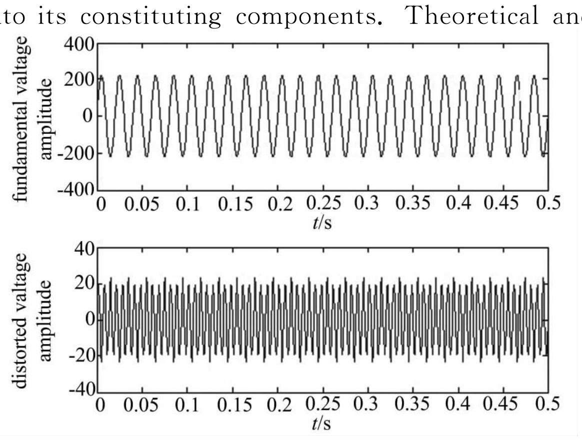

Fig. 7 Fundamental and distort voltage signal wave by using proposed method

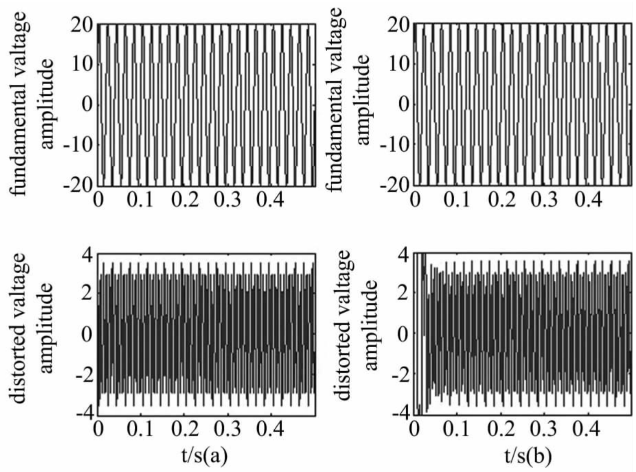

Fig. 8 Fundamental and distort current signal wave by using proposed method

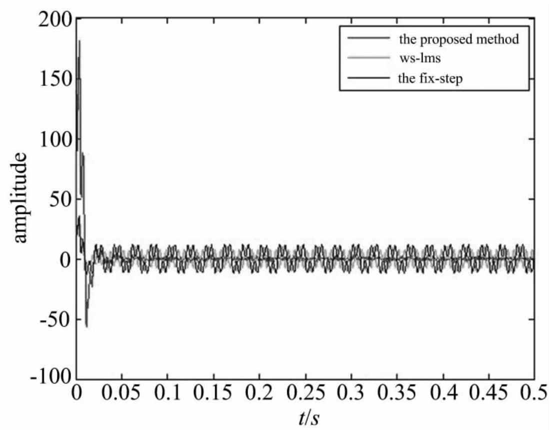

Fig. 9 $e(k)$ in the proposed method, WV-LMS and the fix-step

simulation studies verify the effectiveness of the proposed method.

Tab. 1 Calculate result of power in proposed method

sinal	theoretical value	measure	value error
P_1	2 200	2 200	0
P_d	30.75	30.749 9	-2.05×10^{-11}

Tab. 2 Calculate result of power in fixed LMS

sinal	theoretical value	measure value	error
P1	2 200	2 199.999 9	-3.04×10^{-4}
Pd	30.75	30.749 9	-2.05×10^{-5}

Tab. 3 Calculate result of power in ws-LMS

sinal	theoretical value	measure value	error
P_1 2 200	2 199.99	-4.04×10^{-6}	—
P_d	30.75	30.74	-5.05×10^{-7}

References

[1] 庞浩,李东霞,俎云霄,等. 应用 FFT 进行电力系统谐波分析的改进算法[J]. 中国电机工程学报,2003,23(6):50-54.
Pang H, Li D X, Zu Y X, et al. An improved algorithm for harmonic analysis of power system using FFT technique[J]. Proceedings of the CSEE, 2003, 23(6): 50-54.

[2] Zhang F S, Geng Z X, Yuan W. The algorithm of interpolating windowed FFT for harmonic analysis of electric power system[J]. IEEE Transactions on Power Delivery, 2001, 16(2): 160-164.

[3] Mojiri M, Karimi-Ghartemani M, Bakhshai A. Time-domain signal analysis using adaptive notch filter[J]. IEEE Transactions on Signal Processing, 2007, 55(1): 85-93.

[4] 刘欢,褚建新,俞万能. 改进型自适应陷波器电力系统频率估计方法[J]. 上海海事大学学报, 2007, 28(3): 24-27.
Liu H, Chu J X, Yu W N, Accurate estimation of power system frequency using a modified adaptive notch filter [J]. Joumal of Shanghai Maritime University, 2007, 28(3): 24-27.

[5] Yazdekhasti A, Mojiri M. A method for harmonic extraction from power systems signals based on adaptive notch filter[J]. Advances in Computational Mathematics and its Applications, 2012, 1(1): 40-46.

[6] Chien W C, Lin C M, Singh P K, et al. MMIC compact filters with third harmonic suppression for V-band applications [J]. Microwave and Wireless Components Letters, 2011, 21(6): 295-297.

[7] 薛蕙,罗红. 小波变换与傅里叶变换相结合的暂态谐波分析方法[J]. 中国农业大学学报, 2007, 12(6): 89-92.
Xue H, Luo H. Transient harmonic analysis algorithm using wavelet transform and Fourier transform [J]. Journal of China Agricultural University, 2007, 12(6): 89-92.

[8] Nguyen N, Milanfar P. A wavelet-based interpolation restoration method for superresolution (wavelet superresolution) [J]. Circuits, Systems and Signal Processing, 2000, 19(4): 321-338.

[9] Stephanakis I M, Kollias S. Optimal wavelet filter banks for regularized restoration of noisy images [J]. Circuits, Systems and Signal Processing, 2000, 19(2): 99-119.

[10] 郑军，颜文俊，诸静. 基于尺度滤波与小波去噪的 PID 继电整定[J]. 控制与决策，2005，20(7)：811-814,833.
Zheng J, Yan W J, Zhu J. Relay auto-turning for PID control based on scale filter and wavelet denoising [J]. Control and Decision, 2005, 20(7): 811-814,833.

[11] 张玉璘，陈伟民，杨建春，等. 小波变换自适应滤波器及其在主动噪声控制中的应用[J]. 控制与决策，2002，17(1)：107-110.
Zhang Y L, Chen W M, Yang J C, et al. Wavelet transformation adaptive filter and its application in active noise control [J]. Control and Decision, 2002, 17(1): 107-110.

[12] 倪元敏，张晓冰. 畸变信号条件下电能合理计量方法探讨[J]. 电力系统自动化，2008，32(17)：88-91.
Ni Y M, Zhang X B. Research on a new method of rational electric energy measurement under the distorted signals condition [J]. Automation of Electric Power Systems, 2008, 32(17): 88-91.

[13] Wakileh G J. 电力系统谐波--基本原理、分析方法和滤波器设计[M]. 徐证译，北京：机械工业出版社，2003.

[14] Maragos P, Kaiser J F, Quatieri T F. Energy separation in signal modulations with application to speech analysis [J]. IEEE Transactions on Signal Processing, 1993, 41(10): 3024-3051.

[15] Sristi P, Lu W S, Antoniou A. A new variable-step-size LMS algorithm and its application in subband adaptive filtering for echo cancellation [J]. IEEE International Symposium on Circuits and Systems, 2012, 2: 721-724.

（上接第 835 页）

[9] Pan G, Qi G D, Zhang W S, et al. Trace analysis and mining for smart cities: Issues, methods, and applications [J]. IEEE Communications Magazine, 2013, 51(6): 120-126.

[10] Zadegan S M R, Mirzaie M, Sadoughi F. Ranked k-medoids: A fast and accurate rank-based partitioning algorithm for clustering large datasets [J]. Knowledge-Based Systems, 2013, 39:133-143.

[11] Wu O, Hu W M, Maybank S J, et al. Efficient clustering aggregation based on data fragments [J]. IEEE Transactions on Systems, Man, and Cybernetics, 2012, 42(3): 913-926.

[12] Shi J M, Mamoulis N, Wu D M, et al. Density-based place clustering in geo-social networks[C]// Proceedings of the ACM SIGMOD International Conference on Management of Data. Snowbird, USA: ACM Press, 2014: 99-110.

[13] Liu S Y, Liu Y H, Ni L M, et al. Towards mobility-based clustering [C]// Proceedings of the 16th ACM SIGKDD International Conference on Knowledge Discovery and Data Mining. Washington, USA: ACM Press, 2010: 919-928.

[14] Dai J. A novel moving object trajectories clustering approach for very large datasets[C]// Proceedings of the 2nd International Conference on Computer Science and Electronics Engineering. Paris, France: Atlantis Press, 2013: 863-866.

[15] Patel J M, Chen Y, Chakka V P. STRIPES: An efficient index for predicted trajectories[C]// Proceedings of the ACM SIGMOD International Conference on Management of Data. Paris, France: ACM Press, 2004:635-646.

[16] Mamoulis N, Cao H P, Kollios G, et al. Mining, indexing, and querying historical spatiotemporal data[C]// Proceedings of the tenth ACM SIGKDD International Conference on Knowledge Discovery and Data Mining. Seattle, USA: ACM Press, 2004: 236-245.

[17] Jensen C S, Lin D, Chin B, et al. Effective density queries on continuously moving objects[C]// Proceedings of the 22nd International Conference on Data Engineering. Atlanta, USA: IEEE Computer Society, 2006: 1-11.

[18] 刘奎恩，丁治明，李明树. MOIR/HR：覆盖区域受限的热门区域挖掘[J]. 计算机研究与发展，2010，47(z1)：455-458.
Liu K E, Ding Z M, Li M S. MOIR/HR: Mining of hot regions with coverage constraints[J]. Journal of Computer Research and Development, 2010, 47(z1): 455-458.

[19] Worton B J. Kernel methods for estimating the utilization distribution in home-range studies[J]. Ecology, 1989: 70(1):164-168.